RESEARCH ARTICLE

Single-Input Multiple-Output K-Complex Symbol Golden Codeword Media-Based Modulation

NARUSHAN PILLAY AND **HONGJUN XU**, (Member, IEEE)

School of Engineering, University of KwaZulu-Natal, Durban 4041, South Africa

Corresponding author: Narushan Pillay (pillayn@ukzn.ac.za)

ABSTRACT The K-complex symbol Golden codeword-based modulation (KCSGC) scheme for multiple-input multiple-output systems has been recently proposed in the literature and is capable of achieving a high diversity order by transmitting the same K complex symbols in each of K time slots. In this paper, we investigate improving the spectral efficiency of a single-input multiple-output (SIMO) configuration of the scheme (SIMO-KCSGC) by employing radio frequency (RF) mirror assisted media-based modulation (MBM). Three schemes are investigated: Scheme 1 employs the same RF mirror activation pattern (MAP) in each of K time slots, Scheme 2 employs different MAPs in each of the K time slots, while Scheme 3 employs different MAPs in a subset k of the K time slots. A joint detector based on the sorted symbol set sphere decoder and maximum-likelihood detection rule is presented and its computational complexity is analyzed. The bit error rate versus signal-to-noise ratio (SNR) curves show that there is a negligible penalty incurred in SNR gain when the spectral efficiency is increased by a few bits per channel use. For higher increases in spectral efficiency, the penalty increases but is less significant with increasing K. Scheme 1 is found to be superior in terms of the error performance-spectral efficiency trade-off. The theoretical average bit error probability is derived for the SIMO-KCSGC-MBM scheme and demonstrates a very close match with simulation results.

INDEX TERMS Golden codes, Golden codeword-based modulation, media-based modulation, mirror activation pattern, multiple complex symbol Golden code, radio frequency mirror, sorted symbol set sphere decoding.

I. INTRODUCTION

Higher spectral efficiency is one of the key demands of the next generation of networks. For example, the 5G standard promises spectral efficiencies between 0.12 and 30 bits/s/Hz and a further increase will be expected for the 6G standard. Consequently, improved techniques and schemes that will render this realizable are attracting vast interest in the research community. Simultaneously, superior reliability (error performance) is an accepted norm in the new generation of standards.

In terms of achieving superior reliability, the Golden code [1] is an extremely attractive scheme since it is capable of achieving both full-rate and full-diversity. However, due to the extremely high computational complexity imposed during

The associate editor coordinating the review of this manuscript and approving it for publication was Yafei Hou.

the detection of the Golden codewords, researchers have considered other schemes that have more practical detection computational complexity. Recently, several contributions which now render key features of the Golden code obtainable have been proposed in [2], [3], and [4]; hence, demanding increased attention. Golden codeword based modulation for single-input multiple-output (SIMO) systems was proposed in [2] to exploit the superior distance properties of the Golden code, while requiring only a single transmit antenna. The scheme transmits Golden codeword super-symbols over two consecutive time-slots and demonstrates an improved error performance with practicable receiver detection complexity. In [3], the concept of [2] is considered together with the application of component interleaving to exploit signal-space diversity. The scheme transmits interleaved Golden codeword super-symbols over four consecutive time-slots to achieve an increased diversity order. Another scheme, which can be

considered as a generalization of the Golden codeword modulation is the K complex symbol Golden codeword (KCSGC) based modulation [4]. The scheme not only exploits the advantages of the Golden code, while employing practicable detection, but also increases the achievable diversity order by an order of K, the number of quadrature amplitude modulation symbols employed in the transmission over the same number of consecutive time slots.

Meanwhile, media-based modulation (MBM) has been recently proposed in the literature [5], [6], [7] and has the potential to address the requirement for higher spectral efficiencies. MBM is able to transmit information by manipulating the far-field radiation pattern of reconfigurable antennas. In MBM, the process of embedding information in the channel states may be realized by switching radio frequency (RF) mirrors co-located around a transmit antenna ON/OFF, while using index modulation to map input information bits to unique channel fade realizations or mirror activation patterns (MAPs) [8]. This allows large gains in spectral efficiency to be achieved [8].

Several recent contributions have been found in the open literature. For example in [9], space-time MBM is proposed. The scheme is based on space-shift keying and employs the Hurwitz-Radon matrix family to realize transmit diversity gain with a single RF chain. In [10], space-time channel modulation (STCM) is proposed. STCM improves upon the spectral efficiency/error performance of the Alamouti space-time block code by exploiting MBM using RF mirrors. Three STCM schemes/configurations were investigated for a quasi-static frequency-flat Rayleigh fading channel, however, while Scheme 3 achieves full-diversity and the superior error performance, Scheme 1 does not provide transmit diversity. On the other hand, Scheme 2 achieves full-diversity with a smaller spectral efficiency, while imposing the lowest complexity maximum-likelihood (ML) detector amongst the three schemes. Meanwhile, the superior error performance of Scheme 3 was achieved at the cost of the highest computational complexity [10]. An analysis of the performance of full-duplex decode-and-forward relaying with MBM was investigated in [11]. The analysis formulates the upper bounds for the end-to-end average bit error probability and derives the achievable diversity order. Furthermore, the upper and lower bounds for the achievable rate are derived. Design of the signal set for MBM to achieve good structured sparse lattice codes in higher dimensions was studied in [12]. The proposed design is capable of achieving higher diversity slopes especially at low- and medium-signal-to-noise ratios (SNRs). MBM was also employed in [13] and [14] to enhance the error performance of quadrature spatial modulation.

Some recent examples have also considered reconfigurable intelligent surfaces (RISs) and MBM. In [15], a combination of MBM and RISs is proposed in the form of non-differential and differential schemes. In the former scheme, phase variations of the RIS are exploited to enhance the achievable data rate, while for the differential scheme, a differential space-time block code MBM RIS-aided scheme is investigated

which does not require channel estimation at the receiver. In [16], a large RIS is investigated for the generation of radiation pattern states required in MBM. Hence, it is shown that MBM can be realized via RISs.

The KCSGC scheme achieves superior error performance due to its achievable diversity order, while the MBM technique can be exploited to significantly improve the spectral efficiency of the KCSGC scheme. Hence, based on the above motivation, we aim to investigate SIMO-KCSGC with MBM, hereinafter referred to as SIMO-KCSGC-MBM. Since transmission takes place over K consecutive time slots[1] we consider different options for mapping input bits to MAPs.

Contributions: Based on the above background and motivation, the contributions of this paper are: a) RF mirror-assisted MBM is applied to the SIMO-KCSGC scheme with the aim of improving spectral efficiency. Three different schemes are investigated. Schemes 1-3 vary based on the manner in which input bits are mapped to the MAPs. b) The theoretical average bit error probability (ABEP) is formulated for the SIMO-KCSGC-MBM scheme, and c) sphere decoding based detection is devised for the scheme and its computational complexity is analyzed.

Organization: The remainder of the paper is organized as follows: In Section II, we present the system model of the SIMO-KCSGC-MBM scheme including an example of the encoding for $K = 4$ and MBM related mapping. Furthermore, the formulation of the ABEP, detection at the receiver based on a joint sorted symbol set sphere decoding and ML detection rule and its complexity analysis are presented. Section III presents the numerical results, while concluding remarks are drawn in Section IV.

Notation: Upper-case bold symbols represent sets or matrices, while lower-case bold symbols represent vectors. $|\cdot|$, $\|\cdot\|_F$, $(\cdot)^T$ and $(\cdot)^H$ represents the Euclidean norm, Frobenius norm, transpose and Hermitian, respectively. $E\{\cdot\}$ is the expectation operator, while $\mathcal{D}(\cdot)$, $Q(\cdot)$ represents the constellation demodulation function and Gaussian Q-function, respectively. $\text{argsort}(\boldsymbol{\Theta})$ returns the set of indices corresponding to the elements of $\boldsymbol{\Theta}$ sorted in ascending order. $(\cdot)!$ represents factorial and $\text{argmin}_\epsilon(f(\epsilon))$ represents the value of ϵ for which $f(\epsilon)$ attains its minimum. j is the complex number $\sqrt{-1}$. $\Re\{\cdot\}$ represents the real part of an argument.

II. SIMO-KCSGC-MBM
A. SYSTEM AND EQUIVALENT RECEIVED SIGNAL MODELS
Consider a SIMO system with a single antenna at the transmitter surrounded by n_{rf} RF mirrors and N_r antennas at the receiver as depicted in Figure 1. The n_{rf} mirrors generates $N_{rf} = 2^{n_{rf}}$ MAPs. Given an input bit stream of $n_b = n_{b_1} + n_{b_2}$ bits, n_{b_1} bits are mapped to K M-ary quadrature amplitude modulation (MQAM) symbols and the remaining n_{b_2} bits yield k, $k \in [1 : K]$ mappings each from N_{rf} MAPs based on one of three schemes employed, where $n_{b_1} = K \log_2 M$ and $n_{b_2} = k \log_2 N_{rf}$. Scheme 1 employs the same MAP over

---

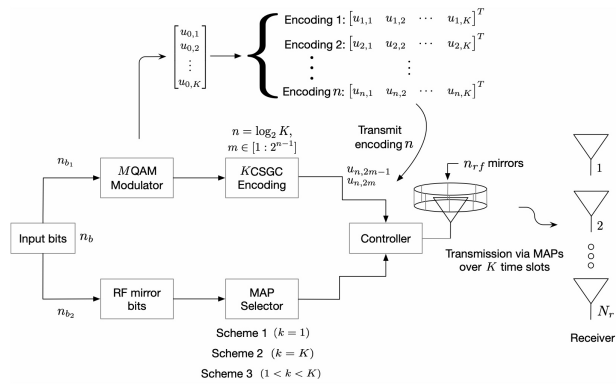[1]In this paper, we consider only $K = 2$, 4 and 8.

FIGURE 1. System model of SIMO-KCSGC-MBM.

FIGURE 2. Comparison of spectral efficiency δ versus number of RF mirrors n_{rf} for Schemes 1-3 with $K = 2$, 4 and 8.

K consecutive time slots, Scheme 2 employs different MAPs over K consecutive time-slots, while Scheme 3 employs different MAPs over a subset k, $k \in [2 : K - 1]$ of the K time slots. The spectral efficiency in bits per channel use (bpcu) can therefore be defined as:

$$\delta = \log_2 M + \frac{k}{K} \log_2 N_{rf}, \quad (1)$$

where $k = 1$ for Scheme 1, $k = K$ for Scheme 2 and $1 < k < K$ in the case of Scheme 3.

The corresponding curves for δ with different settings of k are shown in Figure 2. For $K = 2$, 4 and 8, as expected, it is evident that Scheme 2 provides the highest increase in spectral efficiency compared to KCSGC, followed by Schemes 3 and 1. However, inherently, there will exist a trade-off between the error performance and achievable spectral efficiency.

The MQAM symbols are then sent to the KCSGC encoding unit which generates super-symbols of the form $u_{n,2m-1}$ and $u_{n,2m}$ at the n-th, $n = \log_2 K$, encoding defined as:

$$u_{n,2m-1} = \frac{1}{\sqrt{5}} \alpha (u_{n-1,m} + u_{n-1,m+2^{n-1}} \theta), \quad (2.1)$$

$$u_{n,2m} = \frac{1}{\sqrt{5}} \bar{\alpha} (u_{n-1,m} + u_{n-1,m+2^{n-1}} \bar{\theta}), \quad (2.2)$$

where $m \in [1 : 2^{n-1}]$, $\theta = \frac{1+\sqrt{5}}{2}$, $\bar{\theta} = 1 - \theta$, $\alpha = 1 + j\bar{\theta}$, $\bar{\alpha} = 1 + j\theta$ and $[u_{0,1}, u_{0,2}, \cdots, u_{0,K}]$ are the K transmitted MQAM symbols.

The super-symbols are then transmitted over K consecutive time slots with the MAP activations as described previously. An example of the encoding is given in the subsequent subsection.

Assuming a Rayleigh frequency-flat fading channel which changes every time slot, the corresponding received signal vector of dimension $N_r \times 1$ is then given as:

$$\mathbf{y}_i = \mathbf{H}_i \mathbf{e}_{\hat{j}_i} u_{n,i} + \boldsymbol{\eta}_i, i \in [1 : K], \quad (3.1)$$

$$= \mathbf{h}_{\hat{j}_i}^i u_{n,i} + \boldsymbol{\eta}_i, \quad (3.2)$$

where $\mathbf{H}_i$ is the $N_r \times N_{rf}$ channel matrix corresponding to the i-th time slot with independent and identically distributed
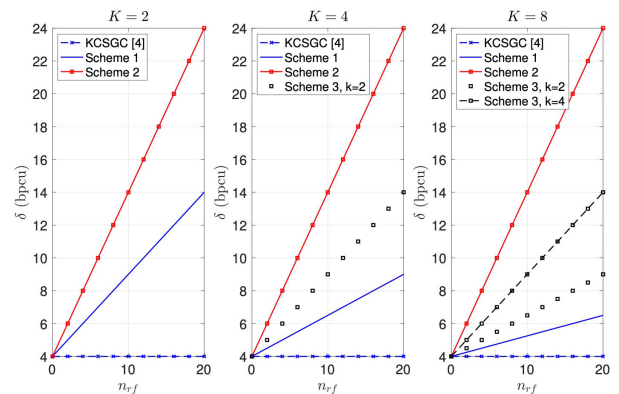
(i.i.d.) entries distributed as $\mathcal{CN}(0, 1)$, $\mathbf{e}_{\hat{j}_i}$ is the $N_{rf} \times 1$ vector, with a single non-zero unit entry at the mapped position $\hat{j}_i$, $j_i \in [1 : N_{rf}]$ for the i-th time slot, the product of $\mathbf{H}_i \mathbf{e}_{\hat{j}_i}$ is $\mathbf{h}_{\hat{j}_i}^i$ which represents an $N_r \times 1$ column vector of $\mathbf{H}_i$ with column index $\hat{j}_i$ and $\boldsymbol{\eta}_i$ is the $N_r \times 1$ vector representing additive white Gaussian noise (AWGN) with i.i.d. entries distributed as $\mathcal{CN}(0, \frac{1}{\gamma})$, with γ the average SNR per receive antenna. For Scheme 1, $k = 1$ and $\hat{j}_1 = \hat{j}_2 = \cdots = \hat{j}_K$, thus $\mathbf{e}_{\hat{j}_1} = \mathbf{e}_{\hat{j}_2} = \cdots = \mathbf{e}_{\hat{j}_K}$. For Scheme 2, $k = K$; hence, n_{b_2} inputs bits are independently mapped to the set of indices $\{\hat{j}_1, \hat{j}_2, \cdots, \hat{j}_K\}$ resulting in the set of vectors $\{\mathbf{e}_{\hat{j}_1}, \mathbf{e}_{\hat{j}_2}, \cdots, \mathbf{e}_{\hat{j}_K}\}$. In the case of Scheme 3, $1 < k < K$; hence, $\hat{j}_1 = \hat{j}_2 = \cdots = \hat{j}_k$ and $\mathbf{e}_{\hat{j}_1} = \mathbf{e}_{\hat{j}_2} = \cdots = \mathbf{e}_{\hat{j}_k}$.

An equivalent received signal model may be derived by representing the K received signal vectors in (3), in a stacked form such that:

$$\bar{\mathbf{y}} = \bar{\mathbf{H}} \mathbf{u} + \bar{\mathbf{n}}, \quad (4)$$

where $\bar{\mathbf{y}} = \begin{bmatrix} \mathbf{y}_1 & \mathbf{y}_2 & \cdots & \mathbf{y}_K \end{bmatrix}^T$ is of dimension $KN_r \times 1$, $\bar{\mathbf{H}}$ is the $KN_r \times K$ channel gain matrix defined as (5), shown at the bottom of the next page, $\mathbf{u} = \begin{bmatrix} u_{0,1} & u_{0,2} & \cdots & u_{0,K} \end{bmatrix}^T$ is of dimension $K \times 1$ and $\bar{\mathbf{n}} = \begin{bmatrix} \boldsymbol{\eta}_1 & \boldsymbol{\eta}_2 & \cdots & \boldsymbol{\eta}_K \end{bmatrix}^T$ is of dimension $KN_r \times 1$. The equivalent received signal model in (4) will be employed in Subsection C to derive the ABEP. The joint detection based on sphere decoding and the ML detection rule with the same model is presented in Subsection D.

B. EXAMPLE OF KCSGC ENCODING FOR $K = 4$ AND MBM MAPPINGS

The key idea in the KCSGC encoding is to transmit the same K symbols in each of the K time slots. This consequently allows a K-fold increase in the diversity order. As an example of the encoding, consider $K = 4$, then with $n = 2$, we have the following super-symbols after the first and second encodings using (2.1) and (2.2):

$$u_{1,2m-1} = \frac{1}{\sqrt{5}} \alpha (u_{0,m} + u_{0,m+2} \theta), \quad (6.1)$$

TABLE 1. Summary of encoding for $K = 4$.

Symbols from 2nd encoding	Symbols from 1st encoding
$u_{2,1} = \frac{1}{\sqrt{5}}\alpha(u_{1,1} + u_{1,3}\theta)$	$u_{1,1} = \frac{1}{\sqrt{5}}\alpha(u_{0,1} + u_{0,3}\theta)$
$u_{2,2} = \frac{1}{\sqrt{5}}\bar{\alpha}(u_{1,1} + u_{1,3}\bar{\theta})$	$u_{1,2} = \frac{1}{\sqrt{5}}\bar{\alpha}(u_{0,1} + u_{0,3}\bar{\theta})$
$u_{2,3} = \frac{1}{\sqrt{5}}\alpha(u_{1,2} + u_{1,4}\theta)$	$u_{1,3} = \frac{1}{\sqrt{5}}\alpha(u_{0,2} + u_{0,4}\theta)$
$u_{2,4} = \frac{1}{\sqrt{5}}\bar{\alpha}(u_{1,2} + u_{1,4}\bar{\theta})$	$u_{1,4} = \frac{1}{\sqrt{5}}\bar{\alpha}(u_{0,2} + u_{0,4}\bar{\theta})$

$$u_{1,2m} = \frac{1}{\sqrt{5}}\bar{\alpha}(u_{0,m} + u_{0,m+2}\bar{\theta}), \quad (6.2)$$

$$u_{2,2m-1} = \frac{1}{\sqrt{5}}\alpha(u_{1,m} + u_{1,m+2}\theta), \quad (6.3)$$

$$u_{2,2m} = \frac{1}{\sqrt{5}}\bar{\alpha}(u_{1,m} + u_{1,m+2}\bar{\theta}). \quad (6.4)$$

The resulting super-symbols for $m \in [1 : 2]$, are then tabulated in Table 1.

Given the transmission of $u_{2,i}$, $i \in [1 : 4]$, since the pairs $\{u_{1,1}, u_{1,3}\}$ and $\{u_{1,2}, u_{1,4}\}$ each carries all the input symbols $u_{0,i}$, every input symbol experiences K fading channels over K time slots. As indicated earlier, this key feature enables an increase in the achievable diversity order.

As an example, the mapping of the n_{b_2} input bits to MAPs for each time slot is shown in Table 2 (refer to the top of Page 5) for $K = 4$. We consider two example input bit streams for each scheme. The status of RF mirrors and formation of the vector $\boldsymbol{e}_{\hat{j}_i}$ are also included.

C. THEORETICAL AVERAGE BIT ERROR PROBABILITY

In the SIMO-KCSGC-MBM scheme, transmission of information is performed by: a) The n-th encoding based on Golden codeword-based symbols, and b) channel modulation via MAPs. Consequently, the average probability of bit error

TABLE 2. Mapping example for the MBM-based scheme $K = 4$, $k = 2$ (Scheme 3).

Scheme	n_{b_2} input bits	Time slot	Mirror status - ON(OFF) (Mirror 1/Mirror 2)	$\hat{j}_i$	$\boldsymbol{e}_{\hat{j}_i}$
			$m_{rf} = 2$, $N_{rf} = 4$, Scheme 1 = 2 bits, Scheme 2 = 8 bits, Scheme 3 = 4 bits		
1	00	1	OFF/OFF	1	$[1\ 0\ 0\ 0]^T$
		2	OFF/OFF	1	$[1\ 0\ 0\ 0]^T$
		3	OFF/OFF	1	$[1\ 0\ 0\ 0]^T$
		4	OFF/OFF	1	$[1\ 0\ 0\ 0]^T$
	10	1	ON/OFF	3	$[0\ 0\ 1\ 0]^T$
		2	ON/OFF	3	$[0\ 0\ 1\ 0]^T$
		3	ON/OFF	3	$[0\ 0\ 1\ 0]^T$
		4	ON/OFF	3	$[0\ 0\ 1\ 0]^T$
2	00110101	1	OFF/OFF	1	$[1\ 0\ 0\ 0]^T$
		2	ON/ON	4	$[0\ 0\ 0\ 1]^T$
		3	OFF/ON	2	$[0\ 1\ 0\ 0]^T$
		4	OFF/ON	2	$[0\ 1\ 0\ 0]^T$
	10101111	1	ON/OFF	3	$[0\ 0\ 1\ 0]^T$
		2	ON/OFF	3	$[0\ 0\ 1\ 0]^T$
		3	ON/ON	4	$[0\ 0\ 0\ 1]^T$
		4	ON/ON	4	$[0\ 0\ 0\ 1]^T$
3	0001	1	OFF/OFF	1	$[1\ 0\ 0\ 0]^T$
		2	OFF/OFF	1	$[1\ 0\ 0\ 0]^T$
		3	OFF/ON	2	$[0\ 1\ 0\ 0]^T$
		4	OFF/ON	2	$[0\ 1\ 0\ 0]^T$
	0110	1	OFF/ON	1	$[1\ 0\ 0\ 0]^T$
		2	OFF/ON	1	$[1\ 0\ 0\ 0]^T$
		3	ON/OFF	3	$[0\ 0\ 1\ 0]^T$
		4	ON/OFF	3	$[0\ 0\ 1\ 0]^T$

for the scheme, assuming independent error events, is determined by the bit error events in a) and/or b).

Based on the above, in order to simplify the formulation of the ABEP, we break down the analysis into the probability of detection of the MQAM symbols transmitted in the n-th encoding and the probability of detection of the activated MAPs. We denote these probabilities as P_s and P_m, respectively.

$$\bar{\mathbf{H}} = \begin{cases} \frac{1}{\sqrt{5}}\begin{bmatrix} h^1_{\hat{j}_1}\alpha & h^1_{\hat{j}_1}\alpha\theta \\ h^2_{\hat{j}_2}\bar{\alpha} & h^2_{\hat{j}_2}\bar{\alpha}\bar{\theta} \end{bmatrix}, & \text{if } K = 2, \\[3em] \frac{1}{5}\begin{bmatrix} h^1_{\hat{j}_1}\alpha^2 & h^1_{\hat{j}_1}\alpha^2\theta & h^1_{\hat{j}_1}\alpha^2\theta & h^1_{\hat{j}_1}\alpha^2\theta^2 \\ h^2_{\hat{j}_2}\alpha\bar{\alpha} & h^2_{\hat{j}_2}\alpha\bar{\alpha}\bar{\theta} & h^2_{\hat{j}_2}\alpha\bar{\alpha}\theta & h^2_{\hat{j}_2}\alpha\bar{\alpha}\theta\bar{\theta} \\ h^3_{\hat{j}_3}\alpha\bar{\alpha} & h^3_{\hat{j}_3}\alpha\bar{\alpha}\theta & h^3_{\hat{j}_3}\alpha\bar{\alpha}\bar{\theta} & h^3_{\hat{j}_3}\alpha\bar{\alpha}\theta\bar{\theta} \\ h^4_{\hat{j}_4}\bar{\alpha}^2 & h^4_{\hat{j}_4}\bar{\alpha}^2\bar{\theta} & h^4_{\hat{j}_4}\bar{\alpha}^2\bar{\theta} & h^4_{\hat{j}_4}\bar{\alpha}^2\bar{\theta}^2 \end{bmatrix}, & \text{if } K = 4, \\[5em] \frac{1}{5\sqrt{5}}\begin{bmatrix} h^1_{\hat{j}_1}\alpha^3 & h^1_{\hat{j}_1}\alpha^3\theta & h^1_{\hat{j}_1}\alpha^3\theta & h^1_{\hat{j}_1}\alpha^3\theta^2 & h^1_{\hat{j}_1}\alpha^3\theta & h^1_{\hat{j}_1}\alpha^3\theta^2 & h^1_{\hat{j}_1}\alpha^3\theta^2 & h^1_{\hat{j}_1}\alpha^3\theta^3 \\ h^2_{\hat{j}_2}\alpha^2\bar{\alpha} & h^2_{\hat{j}_2}\alpha^2\bar{\alpha}\bar{\theta} & h^2_{\hat{j}_2}\alpha^2\bar{\alpha}\theta & h^2_{\hat{j}_2}\alpha^2\bar{\alpha}\theta\bar{\theta} & h^2_{\hat{j}_2}\alpha^2\bar{\alpha}\theta & h^2_{\hat{j}_2}\alpha^2\bar{\alpha}\theta\bar{\theta} & h^2_{\hat{j}_2}\alpha^2\bar{\alpha}\theta^2 & h^2_{\hat{j}_2}\alpha^2\bar{\alpha}\theta^2\bar{\theta} \\ h^3_{\hat{j}_3}\alpha^2\bar{\alpha} & h^3_{\hat{j}_3}\alpha^2\bar{\alpha}\theta & h^3_{\hat{j}_3}\alpha^2\bar{\alpha}\bar{\theta} & h^3_{\hat{j}_3}\alpha^2\bar{\alpha}\theta\bar{\theta} & h^3_{\hat{j}_3}\alpha^2\bar{\alpha}\theta & h^3_{\hat{j}_3}\alpha^2\bar{\alpha}\theta\bar{\theta} & h^3_{\hat{j}_3}\alpha^2\bar{\alpha}\theta^2 & h^3_{\hat{j}_3}\alpha^2\bar{\alpha}\theta^2\bar{\theta} \\ h^4_{\hat{j}_4}\alpha\bar{\alpha}^2 & h^4_{\hat{j}_4}\alpha\bar{\alpha}^2\bar{\theta} & h^4_{\hat{j}_4}\alpha\bar{\alpha}^2\bar{\theta} & h^4_{\hat{j}_4}\alpha\bar{\alpha}^2\bar{\theta}^2 & h^4_{\hat{j}_4}\alpha\bar{\alpha}^2\theta & h^4_{\hat{j}_4}\alpha\bar{\alpha}^2\theta\bar{\theta} & h^4_{\hat{j}_4}\alpha\bar{\alpha}^2\theta\bar{\theta} & h^4_{\hat{j}_4}\alpha\bar{\alpha}^2\theta\bar{\theta}^2 \\ h^5_{\hat{j}_5}\alpha^2\bar{\alpha} & h^5_{\hat{j}_5}\alpha^2\bar{\alpha}\theta & h^5_{\hat{j}_5}\alpha^2\bar{\alpha}\theta & h^5_{\hat{j}_5}\alpha^2\bar{\alpha}\theta^2 & h^5_{\hat{j}_5}\alpha^2\bar{\alpha}\bar{\theta} & h^5_{\hat{j}_5}\alpha^2\bar{\alpha}\theta\bar{\theta} & h^5_{\hat{j}_5}\alpha^2\bar{\alpha}\theta\bar{\theta} & h^5_{\hat{j}_5}\alpha^2\bar{\alpha}\theta^2\bar{\theta} \\ h^6_{\hat{j}_6}\alpha\bar{\alpha}^2 & h^6_{\hat{j}_6}\alpha\bar{\alpha}^2\bar{\theta} & h^6_{\hat{j}_6}\alpha\bar{\alpha}^2\theta & h^6_{\hat{j}_6}\alpha\bar{\alpha}^2\theta\bar{\theta} & h^6_{\hat{j}_6}\alpha\bar{\alpha}^2\bar{\theta} & h^6_{\hat{j}_6}\alpha\bar{\alpha}^2\bar{\theta}^2 & h^6_{\hat{j}_6}\alpha\bar{\alpha}^2\theta\bar{\theta} & h^6_{\hat{j}_6}\alpha\bar{\alpha}^2\theta\bar{\theta}^2 \\ h^7_{\hat{j}_7}\alpha\bar{\alpha}^2 & h^7_{\hat{j}_7}\alpha\bar{\alpha}^2\theta & h^7_{\hat{j}_7}\alpha\bar{\alpha}^2\bar{\theta} & h^7_{\hat{j}_7}\alpha\bar{\alpha}^2\theta\bar{\theta} & h^7_{\hat{j}_7}\alpha\bar{\alpha}^2\bar{\theta} & h^7_{\hat{j}_7}\alpha\bar{\alpha}^2\bar{\theta}^2 & h^7_{\hat{j}_7}\alpha\bar{\alpha}^2\theta\bar{\theta} & h^7_{\hat{j}_7}\alpha\bar{\alpha}^2\theta\bar{\theta}^2 \\ h^8_{\hat{j}_8}\bar{\alpha}^3 & h^8_{\hat{j}_8}\bar{\alpha}^3\bar{\theta} & h^8_{\hat{j}_8}\bar{\alpha}^3\bar{\theta} & h^8_{\hat{j}_8}\bar{\alpha}^3\bar{\theta}^2 & h^8_{\hat{j}_8}\bar{\alpha}^3\bar{\theta} & h^8_{\hat{j}_8}\bar{\alpha}^3\bar{\theta}^2 & h^8_{\hat{j}_8}\bar{\alpha}^3\bar{\theta}^2 & h^8_{\hat{j}_8}\bar{\alpha}^3\bar{\theta}^3 \end{bmatrix}, & \text{if } K = 8. \end{cases} \quad (5)$$

Hence, the ABEP may be validated as:

$$P_e \geq P_s + P_m - P_s P_m. \tag{7}$$

Next, we consider closed-form expressions for the probabilities P_s and P_m, respectively:

1) CLOSED-FORM EXPRESSION FOR P_s

Making the simplifying assumption that only $u_{0,1}$ is detected in error [4], while the remaining symbols $u_{0,i}$, $i \in [2:K]$ are detected correctly. Using (3)-(4), the received signal is written as:

$$\mathbf{y}_i = \rho_i \mathbf{h}_{j_i}^i u_{0,1} + \boldsymbol{\eta}_i, i \in [1:K], \tag{8}$$

where ρ_i for $K = 2, 4$ and 8 is given as:

$$
[\rho_1 \ \rho_2 \ \cdots \ \rho_K] =
\begin{cases}
\frac{1}{\sqrt{5}}[\alpha \ \bar{\alpha}], & \text{if } K = 2, \\
\frac{1}{5}[\alpha^2 \ \alpha\bar{\alpha} \ \alpha\bar{\alpha} \ \bar{\alpha}^2], & \text{if } K = 4, \\
\frac{1}{5\sqrt{5}}[\alpha^3 \ \alpha^2\bar{\alpha} \ \alpha^2\bar{\alpha} \ \alpha\bar{\alpha}^2 \ \alpha^2\bar{\alpha} \ \alpha\bar{\alpha}^2 \ \alpha\bar{\alpha}^2 \ \bar{\alpha}^3], \\
\qquad \text{if } K = 8.
\end{cases}
\tag{9}
$$

This is equivalent to the transmission of $MQAM$ symbol $u_{0,1}$ over K independently identical fading channels each with transmit power $|\rho_i|^2$. Hence, the derivation is equivalent to the analysis presented in [4], and is given as:

$$
\begin{aligned}
P_s = \frac{a}{c \log_2 M} &\left\{ \frac{1}{2} \prod_{k=1}^{K} \left(\frac{2}{2+|\rho_k|^2 b\gamma} \right)^{N_r} - \left(\frac{a}{2} \right) \right. \\
&\times \prod_{k=1}^{K} \left(\frac{1}{1+|\rho_k|^2 b\gamma} \right)^{N_r} + (1-a) \\
&\left. \times \sum_{i=1}^{c-1} \prod_{k=1}^{K} \left(\frac{s_i}{s_i+|\rho_k|^2 b\gamma} \right)^{N_r} + \sum_{i=c}^{2c-1} \prod_{k=1}^{K} \left(\frac{s_i}{s_i+|\rho_k|^2 b\gamma} \right)^{N_r} \right\},
\end{aligned}
\tag{10}
$$

where $a = 1 - \frac{1}{\sqrt{M}}$, $b = \frac{3}{M-1}$ and $s_i = 2\sin^2(\frac{i\pi}{4c})$ with c the number of iterations required for convergence of the numerical integration.

2) CLOSED-FORM EXPRESSION FOR P_m

We may formulate the channel modulation bit error by employing an upper bound given by the well-known union bound:

$$P_m \leq \frac{1}{2^{\delta} \delta} \sum_{\Omega} \sum_{\hat{\ell},\ell} N(\hat{\ell}, \ell) PEP, \tag{11}$$

where Ω represents the set of all the codewords from the n-th encoding $u_{n,i}$, $i \in [1:K]$, δ is defined by (1), PEP denotes the unconditional pairwise error probability (PEP) and $N(\hat{\ell}, \ell)$ is the number of bit errors between the actual MAP indices setting for $\hat{j}_1, \hat{j}_2, \cdots, \hat{j}_K$ and the detected MAP

indices setting, as tabulated in Table 3 (please refer to Page 6) for Schemes 1-3.

The PEP may be derived as follows:

Beginning with the conditional PEP, PEP_c is formulated as:

$$
\begin{aligned}
PEP_c = P&\left(\sum_{i=1}^{K} \|\mathbf{y}_i - \mathbf{H}_i e_{\hat{j}_i} u_{n,i}\|_F^2 \right. \\
&\left. < \sum_{i=1}^{K} \|\mathbf{y}_i - \mathbf{H}_i e_{\hat{j}_i} u_{n,i}\|_F^2 \right), \\
= P&\left(\sum_{i=1}^{K} \|\boldsymbol{\eta}_i - \mathbf{H}_i (e_{\hat{j}_i} - e_{\hat{j}_i})\|_F^2 < \sum_{i=1}^{K} \|\boldsymbol{\eta}_i\|_F^2 \right), \tag{12}
\end{aligned}
$$

and may then be simplified as:

$$
\begin{aligned}
PEP_c = P&\left(\sum_{i=1}^{K} \Re\{ \boldsymbol{\eta}_i^H (\mathbf{H}_i (e_{\hat{j}_i} - e_{\hat{j}_i}) u_{n,i}) \} > \right. \\
&\left. \frac{1}{2} \sum_{i=1}^{K} \|\mathbf{H}_i (e_{\hat{j}_i} - e_{\hat{j}_i}) u_{n,i}\|_F^2 \right). \tag{13}
\end{aligned}
$$

It is clearly evident that the random variable:

$$\sum_{i=1}^{K} \Re\{ \boldsymbol{\eta}_i^H (\mathbf{H}_i (e_{\hat{j}_i} - e_{\hat{j}_i}) u_{n,i}) \}, \tag{14}$$

has distribution $\mathcal{N}\left(0, \frac{1}{2\gamma} \sum_{i=1}^{K} \|\mathbf{H}_i (e_{\hat{j}_i} - e_{\hat{j}_i}) u_{n,i}\|_F^2 \right)$; hence, (13) may be written as:

$$PEP_c = Q\left(\sqrt{\sum_{i=1}^{K} v_i} \right), \tag{15}$$

where v_i, $i \in [1:K]$ are central chi-squared RVs with $2N_r$ degrees-of-freedom defined as:

$$v_i = \frac{\gamma}{2} \|\mathbf{H}_i (e_{\hat{j}_i} - e_{\hat{j}_i}) u_{n,i}\|_F^2 = \sum_{k=1}^{2N_r} \alpha_{v_i,k}^2, \tag{16}$$

with $\alpha_{v_i,k}^2$ distributed as $\mathcal{N}(0, \sigma_{v_i}^2)$, $i \in [1:K]$ and $\sigma_{v_i}^2 = \frac{\gamma}{4} \| (e_{\hat{j}_i} - e_{\hat{j}_i}) u_{n,i} \|_F^2$.

Integrating the unconditional PEP, we arrive at:

$$PEP = \int_0^{\infty} \int_0^{\infty} Q\left(\sqrt{\sum_{i=1}^{K} v_i} \right) \prod_{i=1}^{K} p_{v_i}(v_i) dv_i, \tag{17}$$

where $p_{v_i}(v_i) = \frac{1}{(2\sigma_{v_i}^2)^{N_r}(N_r-1)!} v_i^{N_r-1} \exp\left(-\frac{v_i}{2\sigma_{v_i}^2} \right)$ [17] and using the well-known approximation $Q(x) \approx \frac{1}{12}e^{-\frac{1}{2}x^2} + \frac{1}{4}e^{-\frac{2}{3}x^2}$, we arrive at:

$$
\begin{aligned}
PEP \approx \frac{1}{12} &\prod_{i=1}^{K} \left(1 + \frac{\gamma}{4} \| (e_{\hat{j}_i} - e_{\hat{j}_i}) u_{n,i} \|_F^2 \right)^{-N_r} \\
+ \frac{1}{4} &\prod_{i=1}^{K} \left(1 + \frac{\gamma}{3} \| (e_{\hat{j}_i} - e_{\hat{j}_i}) u_{n,i} \|_F^2 \right)^{-N_r}. \tag{18}
\end{aligned}
$$

TABLE 3. Loop setting for searching possible MAPs.

Scheme	MAP indices setting	Loop
1	$\hat{j}_1 = \hat{j}_2 = \cdots = \hat{j}_K, \hat{j}_i \in [1 : N_{rf}]$	$\ell, \hat{\ell} \in [1 : N_{rf}]$
2	$\hat{j}_1, \hat{j}_2, \cdots, \hat{j}_K, \hat{j}_i \in [1 : N_{rf}]$	$\ell, \hat{\ell} \in [1 : N_{rf}^K]$
3	$\hat{j}_1 = \hat{j}_2 = \cdots = \hat{j}_k, \hat{j}_i \in [1 : N_{rf}^k]$	$\ell, \hat{\ell} \in [1 : N_{rf}^k]$

D. JOINT SORTED SYMBOL SET SPHERE DECODING AND ML RULE BASED DETECTION

Consider the equivalent received signal model in (4). The detector needs to consider the MAP indices setting and loop setting ℓ for searching the possible MAPs based on the scheme being detected. Refer to Table 3.

Taking the QR decomposition of $\bar{\mathbf{H}}_\ell$, where $\bar{\mathbf{H}}_\ell$ is given by (5) with the indices set as per Table 3, yielding $\bar{\mathbf{H}}_\ell = \mathbf{Q}_\ell \mathbf{R}_\ell$, where $\mathbf{Q}_\ell$ is a $KN_r \times KN_r$ dimension matrix and $\mathbf{R}_\ell = \begin{bmatrix} \mathbf{R}_1^\ell & \mathbf{R}_2^\ell \end{bmatrix}^T$ is a $KN_r \times K$ matrix with $K \times K$ upper-triangular matrix $\mathbf{R}_1^\ell$ with the (m, n)-th entry $r_\ell(m, n)$ and $(KN_r - K) \times K$ zero matrix $\mathbf{R}_2^\ell$. Then multiplying both sides of (4) by $\mathbf{Q}_\ell^H$, we have:

$$\tilde{\mathbf{y}}_\ell = \mathbf{R}_\ell \mathbf{u} + \tilde{\mathbf{n}}_\ell, \qquad (19)$$

where $\tilde{\mathbf{y}}_\ell = \begin{bmatrix} \tilde{\mathbf{y}}_1^\ell & \tilde{\mathbf{y}}_2^\ell \end{bmatrix}^T$ with $\tilde{\mathbf{y}}_1^\ell$ of dimension $K \times 1$, $\tilde{\mathbf{y}}_2^\ell$ of dimension $(KN_r - K) \times 1$ and $\tilde{\mathbf{n}}_\ell = \mathbf{Q}_\ell^H \tilde{\mathbf{n}}$.

In order to determine the transmitted MQAM symbols and activated MAP/s, we may employ sphere decoding based on solving the metric $\|\tilde{\mathbf{y}}_1^\ell - \mathbf{R}_1^\ell \mathbf{u}\|_F^2 \leq \Delta^2$, where Δ is the radius of the sphere, considering the activation of MAPs for each of Schemes 1-3. Finally, the ML rule is used to determine the most likely combination of MAP/s and symbols.

Accordingly, assuming complete knowledge of the channel $\mathbf{H}_i$, the algorithm for the detection may be represented as follows:

Step 1: Construct $\bar{\mathbf{H}}_\ell$ based on $\mathbf{H}_i$, using the MAP indices setting for each possible value of ℓ, and (5).

Step 2: Determine $\tilde{\mathbf{y}}_1^\ell = \begin{bmatrix} \tilde{y}_1^\ell(1) & \tilde{y}_1^\ell(2) \cdots \tilde{y}_1^\ell(K) \end{bmatrix}^T$ using $\bar{\mathbf{H}}_\ell = \mathbf{Q}_\ell \mathbf{R}_\ell$ and $\tilde{\mathbf{y}}_\ell = \mathbf{Q}_\ell^H \tilde{\mathbf{y}}$.

Step 3: Compute the estimates $\tilde{u}_{0,i}^\ell$ of the K MQAM symbols for the ℓ-th MAP:

$$\tilde{u}_{0,i}^\ell = \mathcal{D}(v_i^\ell), i \in [1 : K], \qquad (20)$$

where:

$$v_i^\ell = \begin{cases} \dfrac{\tilde{y}_1^\ell(K)}{r_\ell(K, K)}, & \text{for } i = K, \\ \dfrac{\tilde{y}_1^\ell(i) - \sum_{m=i+1}^K r_\ell(i, m)\tilde{u}_{0,m}^\ell}{r_\ell(i, i)}, & \text{for } i \in [K - 1 : 1]. \end{cases} \qquad (21)$$

Step 4: Compute $\varphi_q^{i,\ell} = |v_i^\ell - u_0^q|^2$, $i \in [1 : K]$, $q \in [1 : M]$, where u_0^q represents the q-th symbol in the MQAM symbol set Ω^M and sort the constellation symbols from the most-to-least probable transmissions [4]:

$$\bar{\Omega}_{i,\ell}^M = \Omega^M(\text{argsort}(\varphi_1^{i,\ell}, \varphi_2^{i,\ell}, \cdots, \varphi_M^{i,\ell})). \qquad (22)$$

Step 5: Detect the K-th transmitted symbol for the ℓ-th MAP, $\hat{u}_{0,K}^\ell$ using the sphere decoding rule:

$$|\tilde{y}_1^\ell(K) - r_\ell(K, K)s_{K,\ell}^{\tilde{q}}|^2 \leq \Delta^2, \qquad (23)$$

TABLE 4. Summary of Euclidean distance based computations imposed by detector of Subsection D.

Step	Complexity
1-3	0
4	$2MKN_\ell$
5	$3LN_\ell \tau_1$
6	$(2N_\ell - N_\ell K + K^2 N_\ell)\tau_2$
7	$5N_\ell N_r K - 5N_\ell N_r - N_\ell K + N_\ell$

where $s_{i,\ell}^{\tilde{q}} \in \bar{\Omega}_{i,\ell}^M$, $\tilde{q} \in [1 : L]$ is chosen with respect to $\tilde{u}_{0,i}^\ell$, with L, $1 < L \leq M$ the number of most probable transmitted symbols chosen during simulation.

Step 6: Detect each of the remaining MQAM symbols for the ℓ-th MAP and $i \in [K - 1 : 1]$ using:

$$|p_i(s_{i,\ell}^{\tilde{q}})|^2 < \Delta^2 - \sum_{m=i+1}^K |p_m(\hat{u}_{0,m}^\ell)|^2, \qquad (24)$$

where $p_K(\hat{u}_{0,K}^\ell) = \tilde{y}_1^\ell(K) - r_\ell(K, K)\hat{u}_{0,K}^\ell$ and $p_i(z) = \tilde{y}_1^\ell(i) - r_\ell(i, i)z - \sum_{m=i+1}^K r_\ell(i, m)\hat{u}_{0,i}^\ell$.

Step 7: Perform detection based on the ML rule to jointly determine the estimations of activated MAPs and transmitted MQAM symbols:

$$[\hat{j}_1 \cdots \hat{j}_K, \tilde{u}_{0,1} \cdots \tilde{u}_{0,K}] = \arg\min_\ell \sum_{i=1}^K \|\mathbf{y}_i - \mathbf{h}_{j_i}^i \hat{u}_{n,i}^\ell\|_F^2, \qquad (25)$$

where:

$$\hat{u}_{n,2m-1}^\ell = \frac{1}{\sqrt{5}}\alpha(\hat{u}_{n-1,m}^\ell + \hat{u}_{n-1,m+2^{n-1}}^\ell \theta), \qquad (26)$$

$$\hat{u}_{n,2m}^\ell = \frac{1}{\sqrt{5}}\bar{\alpha}(\hat{u}_{n-1,m}^\ell + \hat{u}_{n-1,m+2^{n-1}}^\ell \bar{\theta}), \qquad (27)$$

with $m \in [1 : 2^{n-1}]$ and $[\hat{u}_{0,1}^\ell, \hat{u}_{0,2}^\ell, \cdots, \hat{u}_{0,K}^\ell]$ are the K detected MQAM symbols for the ℓ-th MAP.

E. COMPUTATIONAL COMPLEXITY ANALYSIS
1) SIMO-KCSGC-MBM
In order to evaluate the computational complexity of the detector presented in the preceding subsection, we consider the number of Euclidean distance operations required to be evaluated in the algorithm. Only Steps 4-7 require Euclidean distance computations. The number of operations required for each of these steps may be validated as summarized in Table 4.

The variable N_ℓ represents the number of possible MAP indices that need to be searched as per Table 3; hence, we have:

$$N_\ell = \begin{cases} N_{rf}, & \text{if Scheme 1,} \\ N_{rf}^K, & \text{if Scheme 2,} \\ N_{rf}^k, & \text{if Scheme 3.} \end{cases} \qquad (28)$$

Note that in Steps 5 and 6, due to the inequality tests, only a percentage of the complexity will be imposed due to convergence. We have used the variables τ_1 and τ_2 for convenience to denote the percentage of this complexity that may be

TABLE 5. Summary of notations and spectral efficiencies (bpcu) with $N_{rf} = 2^{n_{rf}}$.

Scheme	Notation	Spectral efficiency (bpcu)
SIMO-MBM [5]	$(M, n_{rf}, \delta_{SIMO-MBM})$	$\delta_{SIMO-MBM} = \log_2 M + n_{rf}$
SIMO-KCSGC [4]	$(M, \delta_{SIMO-KCSGC})$	$\delta_{SIMO-KCSGC} = \log_2 M$
Scheme 1	(M, n_{rf}, δ)	$\delta = \log_2 M + \frac{1}{K} \log_2 N_{rf}$
Scheme 2	(M, n_{rf}, δ)	$\delta = \log_2 M + \log_2 N_{rf}$
Scheme 3	(M, n_{rf}, k, δ)	$\delta = \log_2 M + \frac{k}{K} \log_2 N_{rf}$
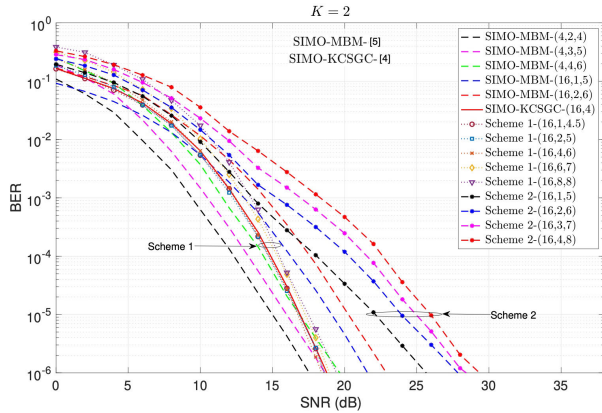
FIGURE 3. Comparison of BER vs. SNR for Schemes 1-3.

imposed. Hence, the overall computational complexity can therefore be expressed as:

$$\tau_{Scheme 1/2/3} = KN_\ell(2M - \tau_2(K+1) + 5N_r - 1)$$
$$+ N_\ell(3L\tau_1 + 2\tau_2 - 5N_r + 1). \quad (29)$$

2) SIMO-MBM

For the SIMO-MBM scheme [5], with 1 transmit antenna employing n_{rf} co-located RF mirrors and N_r receive antennas; assuming a Rayleigh frequency-flat fading channel denoted by the $N_r \times N_{rf}$ matrix **H**, the $N_r \times 1$ received signal vector **y** in the presence of AWGN represented by the $N_r \times 1$ vector **n** can be defined as: $\mathbf{y} = \mathbf{H}\boldsymbol{e}_j u_q + \mathbf{n}$, where u_q, $q \in [1:M]$ is the MQAM symbol transmitted and $\boldsymbol{e}_j$ is the $N_{rf} \times 1$ vector with a single non-zero unit entry at location j, $j \in [1:N_{rf}]$. The entries of **H** and $\boldsymbol{e}_j$ are i.i.d. and distributed as $\mathcal{CN}(0, 1)$.

The corresponding ML detector can be expressed as:

$$[\tilde{j}, \tilde{q}] = \underset{j \in [1:N_{rf}], q \in [1:M]}{\arg\min} \|\mathbf{y} - \mathbf{H}\boldsymbol{e}_j u_q\|_F^2. \quad (30)$$
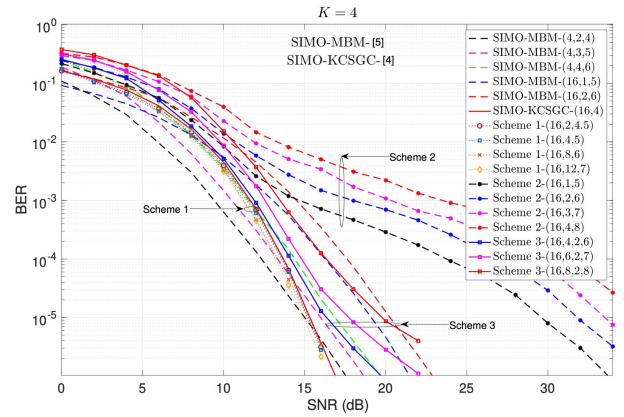
The computational complexity imposed by (30) may be validated as:
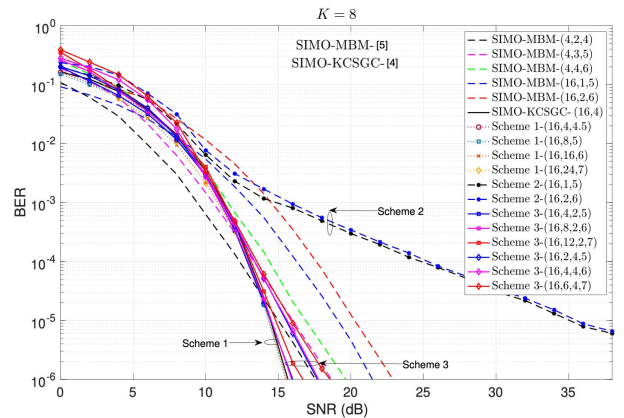
$$\tau_{SIMO-MBM} = (5N_r - 1)N_{rf}M. \quad (31)$$

3) SIMO-KCSGC

For the SIMO-KCSGC scheme, the computational complexity is given by setting $N_\ell = 1$ in (29), and is given as:

$$\tau_{SIMO-KCSGC} = K(2M - \tau_2(K+1) + 5N_r - 1)$$
$$+ 3L\tau_1 + 2\tau_2 - 5N_r + 1. \quad (32)$$

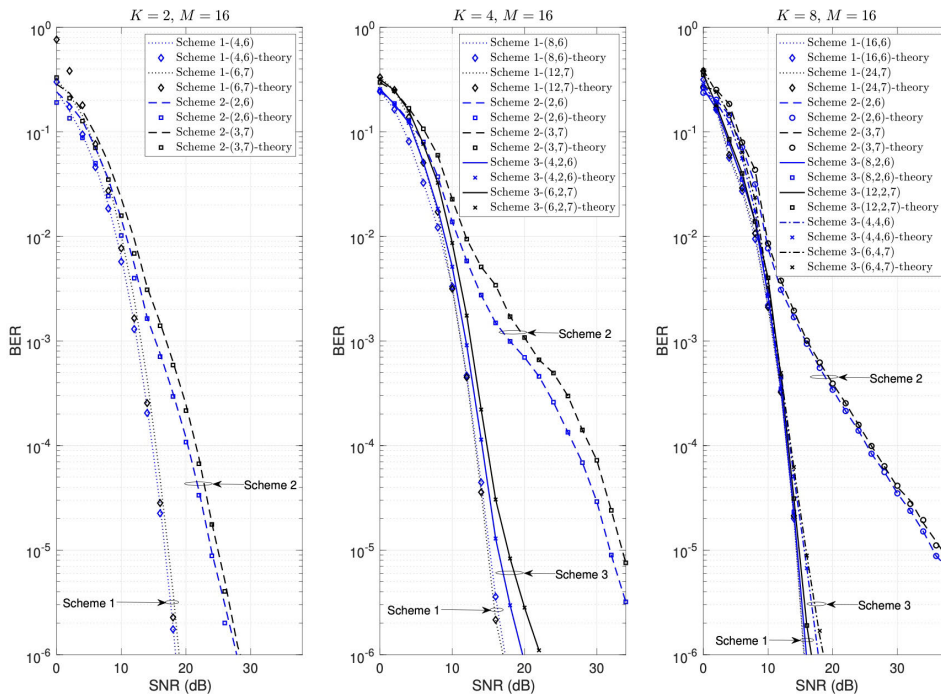**FIGURE 4.** Comparison of BER vs. SNR for Schemes 1-3.

FIGURE 5. Comparison of BER vs. SNR for Schemes 1-3.

In the subsequent section, we draw numerical comparison between the computational complexities given by (29), (31) and (32).

III. NUMERICAL RESULTS

In this section, we first present the numerical results in terms of the average bit error rate (BER) versus average SNR for the proposed SIMO-KCSGC-MBM schemes for $K = 2$, 4 and 8, $M = 16$ and $N_r = 4$. We consider a Rayleigh frequency-flat fading channel which varies from one time-slot to the next. Comparison is drawn with the theoretical ABEP, which was derived in Section II-C, for validation. We consider the primary spectral efficiency of 4 bpcu and vary the number of RF mirrors n_{rf} to yield various spectral efficiencies for Schemes 1-3. We have also included the simulation curves for SIMO-MBM and SIMO-KCSGC. Table 5 summarises the notations and spectral efficiencies for the respective schemes evaluated in this section.

The SIMO-MBM and SIMO-KCSGC schemes have spectral efficiencies $\delta_{SIMO-MBM} = \log_2 M + n_{rf}$ bpcu and $\delta_{SIMO-KCSGC} = \log_2 M$ bpcu, respectively, and will be used for benchmarking purposes. The SIMO-KCSGC curves for 4 bpcu with $K = 2$, 4 and 8 are considered as the reference

FIGURE 6. Comparison of theoretical and simulated average BER vs. average SNR for Schemes 1-3 for $K = 2, 4,$ 8 and $M = 16$.

curves. The values of L assumed in simulations are tabulated in Table 6 (refer to Page 9). We employ the notations $(M, n_{rf}, \delta_{SIMO-MBM})$, $(M, \delta_{SIMO-KCSGC})$ for SIMO-MBM and SIMO-KCSGC, respectively, and (M, n_{rf}, δ), (M, n_{rf}, k, δ) for Schemes 1, 2 and Scheme 3, respectively.

A. AVERAGE BER VERSUS AVERAGE SNR

In this subsection, we present a comparison of simulation results for Schemes 1-3 for $K = 2, 4$ and 8.

Figure 3 presents the error performance results for $K = 2$. Only Schemes 1 and 2 can be evaluated for this setting of K. The SIMO-KCSGC curve for a spectral efficiency of 4 bpcu represents the reference result. SIMO-KCSGC-MBM curves are generated for spectral efficiencies between 4 bpcu and 8 bpcu to evaluate the SNR penalty incurred. For Scheme 1, even at 6 bpcu, there is negligible difference from the reference. For 7 bpcu, an SNR penalty of approximately 0.3 dB is evident. For 8 bpcu, an SNR penalty of approximately 0.8 dB is evident.

Scheme 2 is seen to be significantly inferior to Scheme 1 and the reference by at least 5.2 dB. At 8 bpcu, a penalty of approximately 10 dB is evident. SIMO-MBM is seen as superior in error performance to the reference curves for 4 and 5 bpcu with $M = 4$. It is evident that the diversity order (slope of curve) of the reference curve and Scheme 1 is superior, and for 6 bpcu, SIMO-MBM is inferior by approximately 0.7 dB compared to Scheme 1 (7 bpcu) at a BER of 10^{-6}. We expect that as K increases, the SNR penalties will become

even smaller at a BER of 10^{-6} due to the increasing diversity order.

The results for $K = 4$ are presented in Figure 4 with the reference SIMO-KCSGC curve at 4 bpcu. Schemes 1-3 are all evaluated. Scheme 1 is seen as superior to Schemes 2 and 3. Scheme 1 has been evaluated for various spectral efficiencies up to 7 bpcu. Even at 7 bpcu, the curve matches the reference curve very closely. Once again, it is evident that the Scheme 2 curves are substantially inferior to the reference and at best, for 5 bpcu, is more than 15 dB inferior to the reference result.

For Scheme 3, we have set $k = 2$ and evaluated several curves for spectral efficiencies 6, 7 and 8 bpcu. There is an SNR penalty incurred compared to the reference curve even for 6 bpcu and is approximately 3 dB. For 7 and 8 bpcu, this penalty is increased by 2 and 3 dB, respectively. The SIMO-MBM curves have again been included for comparison. It is evident that Scheme 1 is superior. For example, with 6 bpcu, Scheme 1 is approximately 3 dB superior. The diversity order evident in the slope of the Scheme 1 curve is again higher and even larger SNR gains will be expected at higher SNRs.

The result curves for Schemes 1-3 with $K = 8$ are demonstrated in Figure 5. The SIMO-KCSGC reference curve is once again depicted. Scheme 2 curves depict the same behaviour of inferiority compared to Schemes 1 and 3. For Scheme 1, even at 7 bpcu, there is negligible difference from the reference curve. Scheme 3 is evaluated for $k = 2$ and $k = 4$. The SNR penalties still exist but are smaller as compared to $K = 4$. For 7 bpcu with $k = 2$, a penalty of

TABLE 6. Simulation settings of L for the sorted symbol sphere decoding for SIMO-KCSGC and SIMO-KCSGC-MBM for K = 2, 4, 8 and M = 16.

K	SIMO-KCSGC	SIMO-KCSGC-MBM		
		Scheme 1	Scheme 2	Scheme 3
2	SNR=[0:2:10, 12:2:14, 16, 18:2:20] L=[4, 10, 12, 16]	SNR=[0:2:12, 14, 16:2:18, 20] L=[2, 4, 8, 16]	SNR=[0:2:2, 4, 6:2:12, 14:2:20, 22:2:26, 28:2:30] L=[2, 4, 8, 10, 12, 16]	-
4	SNR=[0:2:10, 12:2:14, 16:2:18] L=[4, 10, 16]	SNR=[0:2:8, 10, 12, 14:2:16, 18] L=[2, 4, 12, 14, 16]	SNR=[0:2:2, 4:2:6, 8:2:16, 18:2:24, 26:2:30] L=[2, 4, 10, 14, 16]	SNR=[0, 2:2:8, 10:2:18, 20:2:24] L=[2, 4, 12, 16]
8	SNR=[0:2:10, 12:2:14, 16] L=[4, 10, 16]	SNR=[0:2:8, 10, 12:2:14, 16] L=[2, 4, 10, 16]	SNR=[0:2:6, 8:2:16, 18:2:26, 28:2:34, 36:2:40] L=[2, 4, 8, 10, 16]	SNR=[0:2:4, 6:2:10, 12:2:16, 18] L=[2, 4, 12, 16]

approximately 1 dB is evident, while for $k = 4$, a penalty of 2.5 dB is seen. Scheme 1 displays the same superior diversity order compared to SIMO-MBM, and for 6 bpcu, there is a gain of approximately 4.5 dB.

1) A SUMMARISING NOTE ON THE COMPARISON WITH SIMO-MBM ERROR PERFORMANCE

Since the SIMO-KCSGC and SIMO-KCSGC-MBM (Scheme 1) schemes exhibit a higher diversity order (slope of error performance curve) than the SIMO-MBM scheme, we can expect that at higher SNRS ($K = 2$) or at higher values of K (moderate-to-high SNRs), their error performance will be superior. In the case of $K = 2$ (refer Figure 3), considering the reference curve for SIMO-KCSGC for 4 bpcu, SIMO-MBM in fact outperforms the reference curve for 4 and 5 bpcu with $M = 4$. However, it is evident that the diversity orders for SIMO-KCSGC and SIMO-KCSGC-MBM (Scheme 1) are higher and we can expect that at higher SNRs there will be a crossover point between the curves. We can also expect that at higher values of K, SIMO-MBM will be inferior due to this feature. As expected, in the case of $K = 4$ and $K = 8$ (refer Figures 4 and 5), and considering the reference curve for SIMO-KCSGC for 4 bpcu, it is immediately evident that the increase in diversity order with increasing K gives the SIMO-KCSGC and SIMO-KCSGC-MBM (Scheme 1) the clear advantage in error performance over the SIMO-MBM scheme.

In Figure 6, we finally draw comparison between the theoretical and simulated error performance results for spectral efficiencies of 6 and 7 bpcu with different settings of n_{rf} and k (Scheme 3). We employ the notation (n_{rf}, δ) for Schemes 1 and 2 and (n_{rf}, k, δ) for Scheme 3. From the results, it is immediately evident that the simulation and theoretical (denoted "theory") curves match well for each of Schemes 1-3.

B. COMPLEXITY

In this subsection, we evaluate the detection computational complexity for the SIMO-KCSGC-MBM, SIMO-MBM [5] and SIMO-KCSGC [4] schemes using the derived formulae given by (29), (31) and (32), respectively. The detection complexities of Schemes 1-3, SIMO-MBM and SIMO-KCSGC are evaluated based on the number of required computations of Euclidean distance imposed by the respective detection algorithms (refer Section II-D and [4, cf. Section IV.B]). We consider spectral efficiencies of 6 bpcu and 7 bpcu. For Schemes 1-3 and SIMO-KCSGC, we consider K = 2, 4 and 8. For each scheme, we use the same settings for L
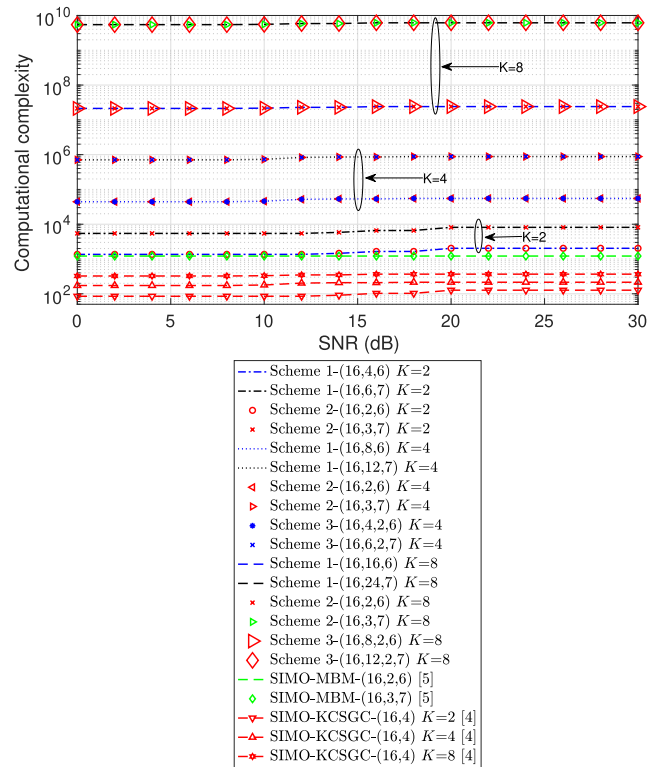
FIGURE 7. Comparison of detection computational complexity vs. average SNR for Schemes 1-3 with K = 2, 4 and 8.

corresponding to each SNR value for ease of comparison and is L = [2, 4, 8, 16], SNR=[0:2:12, 14, 16:2:18, 20:2:30]. We set $\tau_1 = \tau_2 = 0.5$.

From the demonstrated results, it is evident that the complexity of the proposed schemes increases significantly as K is increased. This is expected due to the increase in the number of transmitted symbols per time slot. Furthermore, the complexity in (29) is dominated by the term $KN_\ell M$.

Considering a spectral efficiency of 6 bpcu, at an SNR of 15 dB the complexity of $K = 4$ and $K = 8$ are in the 10^4 and 10^7 orders, respectively, compared to the 10^3 order for $K = 2$. While, for 7 bpcu, at an SNR of 15 dB the complexity of $K = 4$ and $K = 8$ are in the 10^5 and 10^9 orders, respectively, compared to the 10^3 order for $K = 2$.

The computational complexity of the SIMO-MBM scheme is depicted for both 6 and 7 bpcu and is substantially lower than that of the proposed schemes in the order of 10^3. It is further evident that the complexity of the SIMO-KCSGC for $K = 2$, 4 and 8 are all in the 10^2 order and lower than the proposed schemes and SIMO-MBM. For each K, it is found

that the complexity matches for each of the schemes due to the different configuration of RF mirrors employed to achieve the same spectral efficiency. For example, with $K = 4$ and $M = 16$, for a spectral efficiency of 6 bpcu, $N_\ell = 256$ for each of Schemes 1-3.

For the proposed schemes, it is evident that the cost of achieving the higher spectral efficiency is the relatively high computational complexity imposed by the detection, especially for higher values of K. Hence, detectors to further reduce this complexity need to be investigated and will be considered in future work.

IV. CONCLUSION AND FUTURE WORK

In this paper, we have investigated improving the spectral efficiency of the SIMO-KCSGC scheme via the use of RF mirror assisted MBM. Three schemes were proposed that enhance the spectral efficiency by additionally mapping input bits to MAPs in different manners. It was demonstrated that the spectral efficiency of the SIMO-KCSGC scheme can be improved upon by a few bpcu before there is any SNR penalty incurred. Scheme 1 demonstrated a superior error performance-spectral efficiency trade-off; while, for high values of K, Scheme 3 can approach the error performance of Scheme 1. The theoretical ABEP was formulated and shown to match the simulated BER very tightly. Joint sorted symbol sphere decoding and ML based detection was further proposed for the scheme. It was found that the computational complexity is relatively high for higher values of K. Hence, future work involves the investigation of suitable lower complexity detectors.

REFERENCES

[1] J.-C. Belfiore, G. Rekaya, and E. Viterbo, "The golden code: A 2 × 2 full rate space-time code with nonvanishing determinants," *IEEE Trans. Inform. Theory*, vol. 51, no. 4, pp. 1432–1436, Apr. 2005.

[2] H. Xu and N. Pillay, "Golden codeword-based modulation schemes for single-input multiple-output systems," *Int. J. Commun. Syst.*, vol. 32, no. 10, p. e3963, Jul. 2019.

[3] H. Xu and N. Pillay, "The component-interleaved golden code and its low-complexity detection," *IEEE Access*, vol. 8, pp. 59550–59558, 2020.

[4] H. Xu and N. Pillay, "Multiple complex symbol golden code," *IEEE Access*, vol. 8, pp. 103576–103584, 2020.

[5] A. K. Khandani, "Media-based modulation: A new approach to wireless transmission," in *Proc. IEEE Int. Symp. Inf. Theory*, Jul. 2013, pp. 3050–3054.

[6] E. Seifi, A. K. Khandani, and M. Atamanesh, "Media-based modulation for next-generation wireless: A survey and some new developments," 2015, *arXiv:1507.07516*.

[7] Y. Naresh and A. Chockalingam, "On media-based modulation using RF mirrors," *IEEE Trans. Veh. Technol.*, vol. 66, no. 6, pp. 4967–4983, Jun. 2017.

[8] E. Basar, "Media-based modulation for future wireless systems: A tutorial," *IEEE Wireless Commun.*, vol. 26, no. 5, pp. 160–166, Oct. 2019.

[9] Z. Yigit and E. Basar, "Space-time media-based modulation," *IEEE Trans. Signal Process.*, vol. 67, no. 9, pp. 2389–2398, May 2019.

[10] E. Basar and I. Altunbas, "Space-time channel modulation," *IEEE Trans. Veh. Technol.*, vol. 66, no. 8, pp. 7609–7614, Aug. 2017.

[11] Y. Naresh and A. Chockalingam, "Performance analysis of full-duplex decode-and-forward relaying with media-based modulation," *IEEE Trans. Veh. Technol.*, vol. 68, no. 2, pp. 1510–1524, Feb. 2019.

[12] B. Shamasundar and A. Chockalingam, "Constellation design for media-based modulation using block codes and squaring construction," *IEEE J. Sel. Areas Commun.*, vol. 38, no. 9, pp. 2156–2167, Sep. 2020.

[13] I. Yildirim, E. Basar, and I. Altunbas, "Quadrature channel modulation," *IEEE Wireless Commun. Lett.*, vol. 6, no. 6, pp. 790–793, Dec. 2017.

[14] N. Pillay and H. Xu, "Quadrature spatial media-based modulation with RF mirrors," *IET Commun.*, vol. 11, no. 16, pp. 2440–2448, Nov. 2017.

[15] Y. Yan, Y. Cao, and T. Lv, "Enabling media-based modulation for reconfigurable intelligent surface communications," in *Proc. IEEE Wireless Commun. Netw. Conf. (WCNC)*, Mar. 2021, pp. 1–6.

[16] J. A. Hodge, K. V. Mishra, and A. I. Zaghloul, "Media-based modulation with reconfigurable intelligent metasurfaces: Design and performance," in *Proc. IEEE Int. Symp. Antennas Propag. North Amer. Radio Sci. Meeting*, Montreal, QC, Canada, Jul. 2020, pp. 1765–1766.

[17] K. Simon and M.-S. Alouini, *Digital Communication over Fading Channels: A Unified Approach to Performance Analysis*. New York, NY, USA: Wiley, 2000.

NARUSHAN PILLAY received the M.Sc. (Eng.) (cum laude) and Ph.D. degrees in wireless communications from the University of KwaZulu-Natal, South Africa, Durban, in 2008 and 2012, respectively. He has been with the University of KwaZulu-Natal, since 2009. Previously, he was with the Council of Scientific and Industrial Research (CSIR), Defence, Peace, Safety and Security (DPSS), South Africa. His research interests include physical wireless communications, including spectrum sensing for cognitive radio and MIMO systems. He has published several articles in well-known journals in his area of research. He currently supervises several Ph.D. and M.Sc. (Eng.) students. He is also a NRF-rated researcher in South Africa.
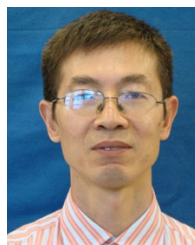
HONGJUN XU (Member, IEEE) received the B.Sc. degree from the Guilin University of Electronic Technology, China, in 1984, the M.Sc. degree from the Institute of Telecontrol and Telemeasure, Shi Jian Zhuang, China, in 1989, and the Ph.D. degree from the Beijing University of Aeronautics and Astronautics, Beijing, China, in 1995. He also did his postdoctoral research with the University of Natal and Inha University, from 1997 to 2000. Currently, he is a Full Professor with the School of Engineering, University of KwaZulu-Natal, Howard College Campus. He is also a national research foundation (NRF) rated researcher in South Africa. He has published more than 50 journal articles. His research interests include digital and wireless communications and digital systems.

• • •